American Journal of Applied Mathematics
2026, Vol. 14, No. 4, pp. 267–276
https://doi.org/10.11648/j.ajam.20261404.19

Research Article

Numerical Simulation of Nonlinear Convective Magnetohydrodynamic Casson-Williamson Fluid Flow over a Wedge with Radiation and Exponential Heat Generation

Doddarasinakere Sreenivasaiah Dhananjaiah[1], Puttaramaiah Prakasha[2], Danagur Kalaiah Jyoti[3,*]

[1]Department of Mathematics, Government First Grade College, Mysore, India
[2]Department of Mathematics, Government First Grade College, Magadi, India
[3]Department of Mathematics, Government College for Women (A), Mandya, India

Abstract

This study examines the nonlinear convective magnetohydrodynamic (MHD) flow and heat transfer characteristics of a Casson-Williamson fluid over a wedge in the presence of nonlinear thermal buoyancy, thermal radiation, a uniform heat source, and exponential internal heat generation. The novelty of the present work lies in the simultaneous integration of the Casson-Williamson non-Newtonian fluid model with nonlinear mixed convection and exponential heat generation over a Falkner-Skan wedge, which has not been comprehensively investigated in previous studies. The nonlinear governing partial differential equations are transformed into a system of coupled ordinary differential equations through appropriate similarity transformations. The resulting boundary value problem is solved numerically using the shooting method in conjunction with the adaptive Runge-Kutta fourth-fifth order (RK45) scheme. The effects of the governing parameters on the velocity and temperature distributions, as well as the skin-friction coefficient and local Nusselt number, are investigated. The numerical results reveal that increasing the Casson and Williamson parameters suppresses the fluid velocity while enhancing the temperature distribution due to reduced convective heat transport. The mixed convection and nonlinear convection parameters accelerate the flow, whereas thermal radiation, uniform heat generation, and exponential heat generation significantly increase the thermal boundary-layer thickness. Moreover, the magnetic field enhances the wall shear stress but reduces the heat transfer rate, while stronger thermal radiation decreases the local Nusselt number. The findings of this investigation provide useful insight into the thermal management of non-Newtonian fluid systems encountered in polymer processing, coating technologies, thermal manufacturing, energy conversion, and related engineering applications.

Keywords

Casson-Williamson Fluid, Falkner–Skan Wedge Flow, Nonlinear Thermal Buoyancy, Exponential Heat Generation

*Correspondence: Danagur Kalaiah Jyoti (jyotidk1510@gmail.com)

Received: 14 July 2026; **Accepted:** 3 August 2026; **Published:** 27 August 2026

Copyright: © The Author(s), 2026. Published by Science Publishing Group. This is an **Open Access** article, distributed under the terms of the Creative Commons Attribution 4.0 License (http://creativecommons.org/licenses/by/4.0/), which permits unrestricted use, distribution and reproduction in any medium, provided the original work is properly cited.

1. Introduction

Many fluids encountered in industrial operations and biological systems cannot be accurately described by the classical Newtonian constitutive law because their viscosity changes with the applied shear rate or they exhibit yield stress before deformation begins. Such materials are collectively referred to as non-Newtonian fluids, and their flow behavior is considerably more complex than that of Newtonian fluids. To capture these rheological characteristics, a variety of constitutive models have been developed over the years. Among the most widely used are the Carreau-Yasuda, Cross, Casson, Maxwell, Powell–Eyring, Prandtl-Eyring, Ellis, Jeffery, and generalized power-law models, each designed to represent specific classes of non-Newtonian materials under different flow conditions [1-3]. These models have provided valuable insights into momentum and heat transfer phenomena in complex fluids and have been successfully applied to numerous engineering problems involving different geometries and boundary conditions. Among these constitutive relations, the Casson fluid model, originally proposed by Casson [4], occupies a prominent position because it effectively describes fluids possessing finite yield stress. According to this model, the fluid behaves as a solid until the applied stress exceeds a critical value, after which it flows like a viscous fluid. This rheological behavior closely resembles that of many real-world materials, including blood, printing inks, chocolate, honey, tomato paste, cosmetic creams, polymer suspensions, and concentrated emulsions. Consequently, the Casson model has found widespread applications in biomedical engineering, food technology, pharmaceutical production, cosmetic processing, and petroleum-related operations. The growing practical importance of Casson fluids has motivated extensive theoretical and numerical investigations. For example, Mukhopadhyay et al. [5] examined the transient boundary-layer flow of a Casson fluid over a stretching surface subjected to specified thermal boundary conditions. Nandeppanavar et al. [6] investigated steady Casson nanofluid flow induced by an exponentially stretching sheet and reported that increasing the Casson parameter suppresses the fluid velocity due to enhanced resistance to deformation. Awais et al. [7] explored magnetohydrodynamic Casson fluid flow through a porous medium over a shrinking surface while considering simultaneous heat and mass transfer effects. Further contributions addressing the transport characteristics of Casson fluids and Casson nanofluids under diverse physical assumptions and thermal environments can be found in Refs. [8-12].

In many thermal transport systems, fluid motion is not governed exclusively by either externally imposed forces or buoyancy effects, but rather by the simultaneous interaction of both mechanisms. This transport regime, commonly known as mixed convection, arises when forced convection and natural convection coexist, resulting in a complex flow behavior that strongly influences momentum and heat transfer characteristics. Such combined convection processes are encountered in a wide variety of engineering applications, including electronic cooling devices, solar thermal systems, thermal energy storage units, nuclear reactors, cryogenic equipment, and numerous manufacturing operations. Owing to its practical importance, mixed convection has become a major area of research, with extensive studies devoted to understanding its influence under different geometrical configurations, fluid models, and thermal boundary conditions [13-20].

Although the classical Boussinesq approximation assumes a linear dependence of fluid density on temperature, this assumption is only valid for relatively small temperature differences. In many practical thermal processes involving significant temperature variations, the density–temperature relationship exhibits nonlinear characteristics, making the linear approximation insufficient for accurately describing buoyancy-driven flows. Consequently, nonlinear thermal buoyancy effects must be incorporated into the governing equations to obtain a more realistic representation of fluid motion and heat transport. The presence of nonlinear convection considerably alters the boundary-layer development and thermal performance, making it highly relevant to applications such as geothermal energy utilization, combustion systems, refrigeration technology, heat pumps, natural gas extraction, and pharmaceutical processing. Several researchers have examined the influence of nonlinear convection in different non-Newtonian fluid models and transport phenomena. Kameswaran et al. [21] investigated the combined effects of nonlinear buoyancy and thermophoretic transport on boundary-layer flow through a permeable medium adjacent to a vertical surface. Hayat et al. [22] analyzed three-dimensional mixed convection flow of a Sisko nanofluid over an elastic stretching sheet by considering both thermal and concentration-induced buoyancy forces. Khan et al. [23] explored entropy generation in the nonlinear mixed convection flow of a tangent hyperbolic nanofluid over an expanding surface and observed that stronger nonlinear buoyancy enhances the fluid velocity. Irfan [24] extended this analysis to magnetohydrodynamic Carreau nanofluid flow with variable thermophysical properties. More recently, further developments on nonlinear mixed convection and its impact on momentum and thermal transport have been reported by Idowu et al. [25], Ibrahim and Kenea [26], Kenea and Ibrahim [27], and Reddy et al. [28].

Despite the extensive literature on Casson fluids, Williamson fluids, mixed convection, and nonlinear thermal buoyancy, very limited attention has been given to the combined effects of the Casson-Williamson non-Newtonian model, nonlinear convection, thermal radiation, a uniform heat source, and exponential internal heat generation over a Falkner-Skan wedge. Most existing investigations consider these physical mechanisms separately or focus on different geometrical configurations. The present study addresses this gap by developing a mathematical model for MHD mixed convection flow and heat transfer of a Casson-Williamson fluid over a wedge and solving the resulting nonlinear equations numerically using the shooting method with the adaptive Runge-

Kutta fourth-fifth order (RK45) scheme. The study provides new insight into the coupled influence of these mechanisms on the velocity field, temperature distribution, wall shear stress, and local Nusselt number.

2. Problem Statement

Consider a steady, two-dimensional boundary-layer flow of an electrically conducting Casson-Williamson fluid past a Falkner–Skan wedge in the presence of an externally imposed transverse magnetic field of uniform strength B_0. The flow is influenced by nonlinear mixed convection arising from temperature-dependent buoyancy, thermal radiation, a uniform internal heat source, and exponential heat generation. Owing to the assumption of a sufficiently small magnetic Reynolds number, the induced magnetic field is neglected in comparison with the applied magnetic field. Furthermore, the effects of viscous dissipation and Joule heating are ignored. Except for the density variation appearing in the buoyancy force, all fluid thermophysical properties are assumed to remain constant, and the density variation is incorporated through the Boussinesq approximation. Here, γdenotes the half-angle of the wedge, while $r$represents the radial coordinate measured along its surface. Based on these assumptions, the governing boundary-layer equations describing the conservation of mass, momentum, and energy are given by

Continuity

$$\frac{\partial(r^m u)}{\partial x}+\frac{\partial(r^m v)}{\partial y}=0. \tag{1}$$

Momentum

$$u\frac{\partial u}{\partial x}+v\frac{\partial u}{\partial y}=\nu\left(1+\frac{1}{\beta}\right)\left(1+\Gamma\frac{\partial u}{\partial y}\right)\frac{\partial^2 u}{\partial y^2}-\frac{\sigma B_0^2}{\rho}u+g[\beta_1(T-T_\infty)+\beta_2(T-T_\infty)^2]\cos\gamma. \tag{2}$$

Energy

$$u\frac{\partial T}{\partial x}+v\frac{\partial T}{\partial y}=\alpha_m\frac{\partial^2 T}{\partial y^2}-\frac{1}{\rho c_p}\frac{\partial q_r}{\partial y}+\frac{Q_t}{\rho c_p}(T-T_\infty)+\frac{Q_e}{\rho c_p}(T_w-T_\infty)\,exp\left(\frac{-n}{l}y\right), \tag{3}$$

The boundary conditions are defined by

$$u=u_w=\frac{\upsilon x}{l^2}, v=0, T=T_w, C=C_w \text{ at } y=0,\ u\to 0, T\to T_\infty, C\to C_\infty \text{ as } y\to 0, \tag{4}$$

here u and v are velocity components along x and y directions respectively, β is the Casson fluid parameter, T and C are temperature and nanoparticles volume fraction respectively, υ is the kinematic viscosity, μ is the dynamic viscosity, σ is the electrical conductivity, ρ density of fluid, B_0 is the magnetic field strength, β_1, β_2 are thermal diffusivities, g is the acceleration due to gravity, $\alpha_m = k/\rho c_p$ is the thermal diffusivity of the fluid, k is the thermal conductivity, c_p is specific heat, $\tau=(\rho c)_p/(\rho c)_f$ is the ratio of the effective heat capacity of nanoparticles and the heat capacity of ordinary fluid, Q_t is the thermal dependent heat source coefficient, Q_e is the exponential space dependent heat source coefficient and q_r is the radiative heat flux.

The energy equation takes the following form in view of Rosseland approximation.

$$u\frac{\partial T}{\partial x}+v\frac{\partial T}{\partial y}=\alpha_m\frac{\partial^2 T}{\partial y^2}+\frac{\partial}{\partial y}\left(\frac{16\sigma^*}{3k^*\rho c_p}T^3\frac{\partial T}{\partial y}\right)+\frac{Q_t}{\rho c_p}(T-T_\infty)+\frac{Q_e}{\rho c_p}(T_w-T_\infty)e^{\frac{-n}{l}y}, \tag{5}$$

where $\sigma^*$and $k^*$are the Stefan-Boltzmann constant and mean absorption coefficient respectively.

Now introduce the stretching transformations

$$\eta=\frac{u_w l}{x\upsilon}y, u=\frac{\upsilon x}{l}f'(\eta), v=\frac{\upsilon(m+1)}{l}f(\eta), T=T_\infty+\theta(\eta)(T_w-T_\infty), \tag{6}$$

here l is characteristic length and prime denotes differentiation with respect to η.

Using (6) in (1)-(5) we have

Hence, the momentum equation is

Now introduce

$$\left(1+\frac{1}{\beta}\right)(1+We\,f'')f'''+(m+1)ff''-(f')^2+Gr(\theta+\alpha_1\theta^2)\cos\gamma-Mf'=0, \tag{7}$$

$$\frac{1+Rd}{Pr}\theta''+(m+1)f\theta'+Q_t\theta+Q_E e^{-n\eta}=0. \tag{8}$$

with the boundary conditions

$$f(0)=0, f'(0)=1, \theta(0)=1,\ f'(\infty)=0, \theta(\infty)=0, \quad (9)$$

In the above equations $Gr, \alpha 1, M, Pr, We, Rd, Qt, QE$, are correspondingly Grashof number, thermal nonlinear convection parameter, magnetic parameter, Prandtl number, Williamson parameter, radiation parameter, thermal dependent heat source/sink parameter and exponential space dependent heat source/sink parameter. They are given below

$$Gr=\frac{gl^2\beta_1(T_w-T_\infty)}{\upsilon u_w}, \alpha_1=\frac{\beta_2(T_w-T_\infty)}{\beta_1}, M=\frac{\sigma B_0^2 l^2}{\rho\upsilon}, Pr=\frac{\upsilon}{\alpha_m}, We=\Gamma U_w\sqrt{\frac{U_w}{\upsilon x}}$$

$$Rd=\frac{16\sigma^* T^3}{3k^* k}, Q_T=\frac{Q_t l^2}{\mu c_p}, Q_E=\frac{Q_e l^2}{\mu c_p}$$

The present study considers only the wedge geometry. Therefore, the governing equations are solved for $m=0$ with $\gamma\neq 0$, representing the steady mixed convective MHD Casson-Williamson fluid flow over a wedge.

The friction factor, Nusselt number and Sherwood number are;

$$C_f=Re_x^{-1/2}\left(1+\frac{1}{\beta}\right)[f''(0)+We(f''(0))^2], \quad (10)$$

$$Nu_x=-\left(1+\frac{4}{3}Rd\right)Re_x^{1/2}\theta'(0), \quad (11)$$

Numerical Procedure

The nonlinear coupled ordinary differential equations (7) and (8), together with the corresponding boundary conditions, are solved numerically using the shooting method combined with the adaptive fourth-fifth order Runge-Kutta (RK45) integration scheme implemented in the Python SciPy library. To facilitate the numerical computation, the higher-order differential equations are first transformed into a system of first-order ordinary differential equations by introducing the following dependent variables:

$$y_1=f, y_2=f', y_3=f'', y_4=\theta, y_5=\theta'.$$

Accordingly, the governing equations are rewritten as

$$\frac{dy_1}{d\eta}=y_2,$$

$$\frac{dy_2}{d\eta}=y_3,$$

$$\frac{dy_3}{d\eta}=\frac{-(m+1)y_1y_3+y_2^2-Gr\left(y_4+\alpha_1 y_4^2\right)\cos\gamma+My_2}{\left(1+\frac{1}{\beta}\right)(1+We\, y_3)}$$

$$\frac{dy_4}{d\eta}=y_5,$$

$$\frac{dy_5}{d\eta}=-\frac{Pr}{1+Rd}[(m+1)y_1y_5+Q_t y_4+Q_E e^{-n\eta}].$$

with the boundary conditions

$$f(0)=0, f'(0)=1, \theta(0)=1,$$

$$f'(\infty)=0, \theta(\infty)=0,$$

The corresponding initial conditions are

$$y_1(0)=0, y_2(0)=1, y_4(0)=1,$$

while the unknown initial slopes

$$y_3(0)=f''(0), y_5(0)=\theta'(0)$$

are determined iteratively using the shooting technique.

The computational domain is truncated to a finite boundary, $\eta_\infty=8$, which is sufficiently large to satisfy the asymptotic boundary conditions. The value of $\eta_\infty=8$ was selected after preliminary computations showed that further enlargement of the computational domain produced negligible changes in the numerical results. Initial guesses are assigned for the unknown quantities $f''(0)$ and $\theta'(0)$. For each set of guessed values, the resulting initial value problem is integrated from $\eta=0$ to $\eta=8$ using the adaptive Runge-Kutta fourth-fifth order (RK45) algorithm. The numerical solution at the far-field boundary is then compared with the required boundary conditions. The nonlinear root-finding algorithm updates the guessed values iteratively until the convergence tolerance of 10^{-6} is achieved, with the stopping criterion given by $|f'(\eta_\infty)|<10^{-6}$ and $|\theta(\eta_\infty)|<10^{-6}$. This ensures that the asymptotic boundary conditions are satisfied with the desired numerical accuracy.

After achieving convergence, the velocity and temperature profiles are obtained for various values of the governing parameters.

To validate the accuracy of the present numerical method, the computed values of the skin-friction coefficient, $(-f''(0))$, are compared with the previously published results of Cortell [29] and Tufail et al. [30] for the special case $(\beta\to\infty), (Gr=0)$, and $(m=0)$. The comparison, presented in Table 1, demonstrates excellent agreement between the present results and the existing literature, thereby confirming the accuracy, stability, and reliability of the numerical procedure employed in this study.

Table 1. Comparison of the present values of the skin-friction coefficient, ($-f''(0)$), with the results of Cortell [29] and Tufail et al. [30] for the special case ($\beta \to \infty$), ($Gr = We = 0$), and ($m = 0$).

M	$-f''(0)$ Cortel [29]	$-f''(0)$ Tufail et al. [30]	$-f''(0)$ Present study	Percentage Error (%)
0	1.00000	1.00000	1.00001	0.0010
0.5	1.22475	1.22474	1.22468	0.0049
1	1.41421	1.41421	1.41414	0.0050
1.5	1.58114	1.58114	1.58105	0.0057
2	1.73205	1.73205	1.73196	0.0052
2.5	-	1.87083	1.87073	0.0053
3	-	2.00000	1.99990	0.0050

Table 2. Effect of M on Skin Friction and Nusselt Number.

M	$-f''(0)$	$-\theta'(0)$
0.5	0.9109990	0.1307026
1	1.04669881	0.0095169
1.5	1.16961929	-0.0095169

(Fixed: $\beta = 2, QE = 0.5, Qt = 0.5, Rd = 0.5, Gr = 0.5, \alpha 1 = 0.5$)

Table 3. Effect of β on Skin Friction and Nusselt Number.

β	$-f''(0)$	$-\theta'(0)$
1	0.93150743	0.1413379
2	1.0466988	0.0095169
3	1.0964163	-0.0489838

(Fixed: $M = 1.0, QE = 0.5, Qt = 0.5, Rd = 0.5, Gr = 0.5, \alpha 1 = 0.5$)

Table 4. Effect of QE on Skin Friction and Nusselt Number.

QE	$-f''(0)$	$-\theta'(0)$
0.1	1.1182457	1.1804138
0.5	1.0466988	0.0095169
1	0.9582551	-1.3358681

(Fixed: β=2, M=1.0, Qt=0.5, Rd=0.5, Gr=0.5, α1=0.5)

Table 5. Effect of Qt on Skin Friction and Nusselt Number.

Qt	$-f''(0)$	$-\theta'(0)$
0.1	1.0870864	0.8216321
0.5	1.0466988	0.0095169
1	0.9385993	-1.7386733

(Fixed: β=2, M=1.0, QE=0.5, Rd=0.5, Gr=0.5, α1=0.5)

Table 6. Effect of Gr on Skin Friction and Nusselt Number.

Gr	$-f''(0)$	$-\theta'(0)$
0.2	1.1667564	-0.0962740
0.5	1.0466988	0.0095169
0.8	0.93505456	0.0917149

(Fixed: β=2, M=1.0, QE=0.5, Qt=0.5, Rd=0.5, α1=0.5)

Table 7. Effect of α1 on Skin Friction and Nusselt Number.

$\alpha 1$	$-f''(0)$	$-\theta'(0)$
0.1	1.0896448	-0.0151034
0.5	1.0466988	0.0095169
0.7	1.0256229	0.0212046

(Fixed: β=2, M=1.0, QE=0.5, Qt=0.5, Rd=0.5, Gr=0.5)

3. Results and Discussion

The influence of the governing dimensionless parameters on the flow and thermal characteristics is examined through a comprehensive numerical investigation. The effects of these parameters on the dimensionless velocity $f'(\eta)$, temperature $\theta(\eta)$, skin-friction coefficient (C_f), and local Nusselt number $(Nu)$are discussed in detail. Unless otherwise specified, the computations are performed using the baseline parameter values $\beta = 2.0, We = 0.5$, $m = 0$, $Gr = 0.8$, $\alpha_1 = 0.7$, $Pr = 6.2$, $Rd = 0.8$, $Q_t = 0.5$, $Q_E = 0.5$, and $n = 1.0$. To isolate the contribution of each physical parameter, only one parameter is varied in each figure while all remaining parameters are held fixed at their reference values. This approach enables a clear assessment of the individual effects of the governing parameters on the momentum and thermal boundary layers, as well as on the surface shear stress and heat transfer rate. Figures 1 and 2 illustrate the influence of the Casson parameter $(\beta)$and the Williamson parameter (We)on the dimensionless velocity profile, respectively. It is evident from Figure 1 that the fluid velocity decreases as the Casson parameter increases. Physically, a larger value of βcorresponds to a fluid with greater resistance to deformation, which weakens the momentum diffusion within the boundary layer. Consequently, the fluid motion is suppressed, leading to a thinner momentum boundary layer and lower velocity throughout the flow region. The effect of the Williamson parameter is presented in Figure 2. The results demonstrate that increasing Wealso reduces the velocity distribution. This behavior is attributed to the enhanced elastic nature of the Williamson fluid, which introduces additional resistance to the flow. As the Williamson parameter increases, the non-Newtonian characteristics become more pronounced, thereby restricting fluid motion and reducing the boundary-layer thickness. Therefore, both the Casson and Williamson parameters act to decelerate the flow, although they originate from different rheological mechanisms: the Casson parameter represents yield-stress effects, whereas the Williamson parameter accounts for shear-thinning viscoelastic behavior. Figures 3 and 4 illustrate the effects of the Casson parameter $(\beta)$and the Williamson parameter (We)on the temperature distribution, respectively. It is observed from Figure 4 that the fluid temperature increases with increasing values of the Casson parameter. Physically, a larger Casson parameter enhances the fluid's yield stress, which suppresses the fluid motion and reduces the convective transport of heat away from the heated surface. Consequently, thermal energy accumulates within the boundary layer, resulting in an increase in the fluid temperature and a thicker thermal boundary layer. Similarly, Figure 4 shows that the temperature profile rises with increasing Williamson parameter. As Weincreases, the non-Newtonian characteristics of the Williamson fluid become more pronounced, offering greater resistance to fluid motion. The weakened convective cooling reduces the rate of heat removal from the surface, allowing more thermal energy to remain within the fluid. This leads to an increase in the temperature distribution and an expansion of the thermal boundary layer.

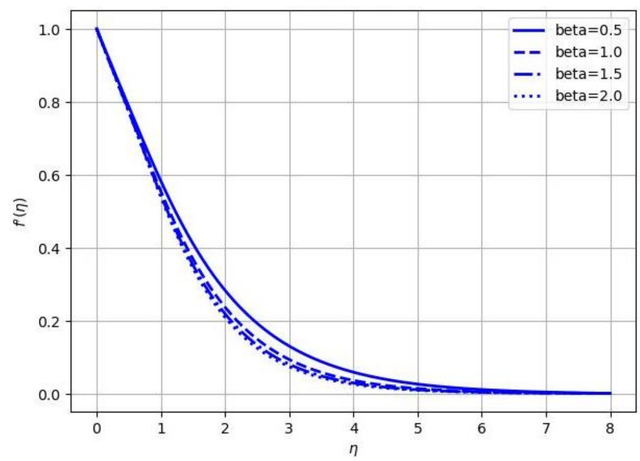

Figure 1. Influence of β on $f'(\eta)$.

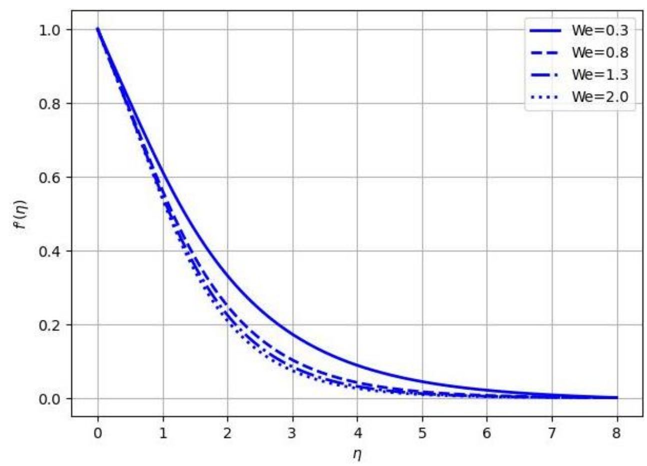

Figure 2. Influence of We on $f'(\eta)$.

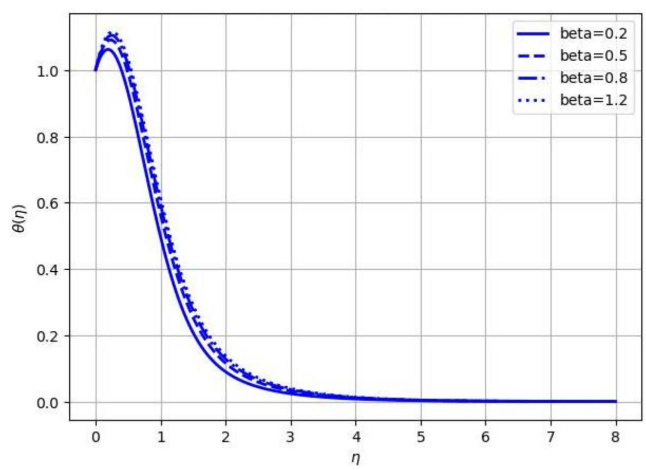

Figure 3. Influence of β on $\theta(\eta)$.

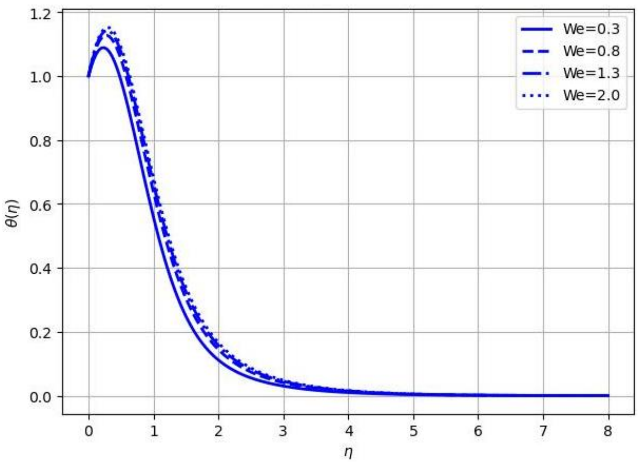

Figure 4*. Influence of* We *on* $\theta(\eta)$.

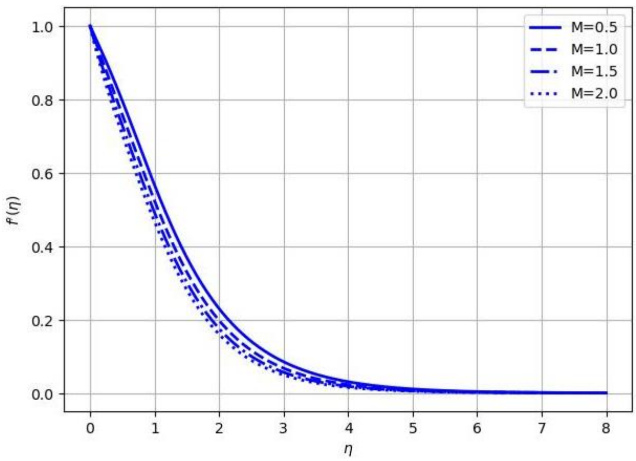

Figure 5*. Influence of* We *on* $f'(\eta)$.

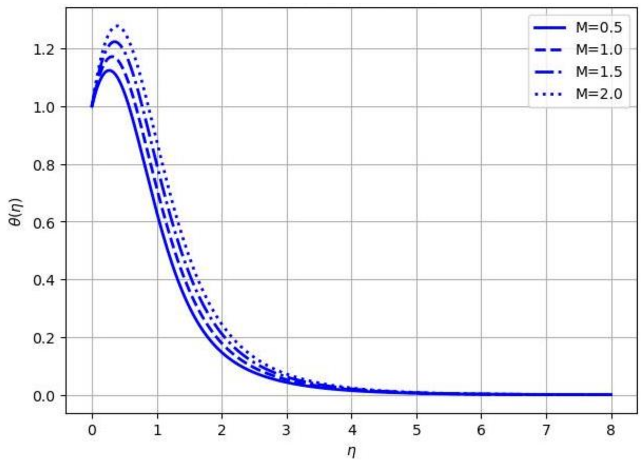

Figure 6*. Influence of M on* $\theta(\eta)$.

Figures 5 and 6 illustrate the effects of the magnetic parameter (M) on the velocity and temperature profiles, respectively. It is observed that increasing (M) decreases the velocity while increasing the temperature. Physically, a stronger magnetic field generates a Lorentz force that opposes the fluid motion, thereby suppressing the velocity and reducing the momentum boundary-layer thickness. The weakened fluid motion diminishes convective heat transfer from the cone surface, causing more thermal energy to be retained within the boundary layer. As a result, the temperature profile and thermal boundary-layer thickness increase with increasing values of the magnetic parameter. Figures 7-9 illustrate the effects of the thermal radiation parameter (R_d), exponential heat generation parameter (Q_E), and uniform heat source parameter (Q_t)on the temperature distribution. It is evident that the temperature profile increases with increasing values of all three parameters. As the thermal radiation parameter increases, additional radiative energy is transferred into the fluid, enhancing the thermal energy within the boundary layer and consequently raising the fluid temperature. Likewise, an increase in the exponential heat generation parameter supplies more internally generated heat to the fluid in an exponentially varying manner, thereby intensifying the temperature field and thickening the thermal boundary layer. A similar trend is observed with the uniform heat source parameter, where larger values of $Q_t$continuously inject thermal energy into the fluid, reducing the rate of cooling and producing higher temperature distributions. Therefore, thermal radiation, exponential heat generation, and uniform heat generation collectively enhance the thermal energy of the fluid, leading to a significant increase in the thermal boundary-layer thickness.

Figures 10 and 11 depict the variations in the skin-friction coefficient for different values of the Casson parameter (β) with changes in the nonlinear convection parameter $(\alpha_1)$and the magnetic parameter (M), respectively. As illustrated in Figure 10, the magnitude of the skin-friction coefficient decreases with increasing values of the Casson parameter, indicating a reduction in the wall shear stress due to the enhanced yield-stress characteristics of the fluid. It is also observed that increasing the nonlinear convection parameter increases the skin-friction coefficient for lower values of the Casson parameter, whereas its influence becomes almost negligible for larger values of β. This behavior is attributed to the stronger buoyancy force generated by nonlinear thermal effects, which enhances the fluid motion near the wedge surface and consequently increases the surface shear. Figure 11 shows that the skin-friction coefficient decreases with increasing magnetic parameter for all values of the Casson parameter. The applied magnetic field generates a Lorentz force that opposes the fluid motion, thereby suppressing the velocity gradient at the wall and reducing the surface shear stress. Moreover, larger values of the Casson parameter further lower the skin-friction coefficient because the increased yield-stress effect offers additional resistance to fluid motion. Tables 2-7 summarize the effects of the governing parameters on the skin-friction coefficient and the local Nusselt number. Table 2 shows that increasing the magnetic parameter (M) enhances the skin-friction coefficient, whereas the local Nusselt number decreases due to the reduction in heat transfer caused by the Lorentz force. Table 3 indicates that larger values of the Casson parameter (β) increase the wall shear stress but reduce the local Nusselt number, reflecting the stronger yield-stress characteristics of the fluid. As observed in Tables 4 and 5, increasing the exponential heat generation parameter (Q_E) and the uniform heat source parameter (Q_t) decreases the skin-friction coefficient while significantly lowering the local Nusselt number, owing to the additional thermal energy generated within the boundary layer. Table 6 demonstrates that increasing the mixed convection parameter (Gr) reduces the skin-friction coefficient, whereas the local Nusselt number increases because stronger buoyancy enhances heat transfer from the wedge surface. Finally, Table 7 reveals that the nonlinear convection parameter (α_1) slightly decreases the skin-friction coefficient while improving the local Nusselt number, indicating enhanced heat transfer under stronger nonlinear buoyancy effects.

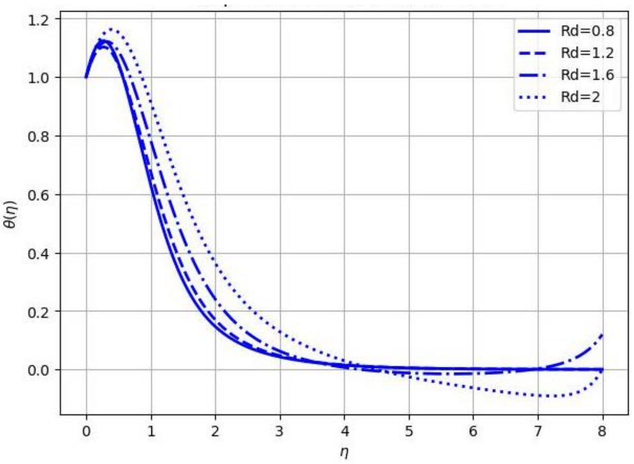

Figure 7. *Influence of* Rd *on* $\theta(\eta)$.

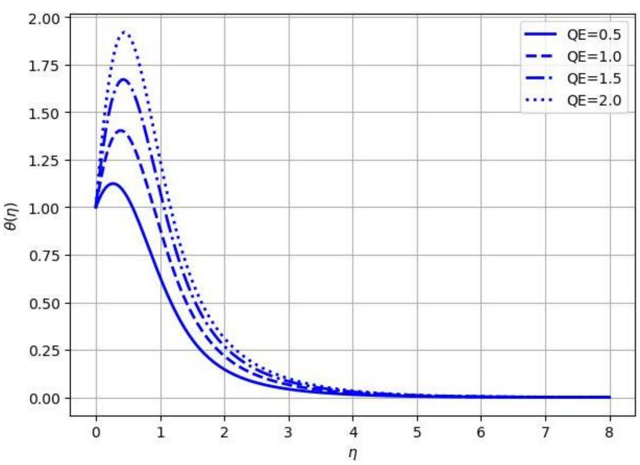

Figure 8. *Influence of* QE *on* $\theta(\eta)$.

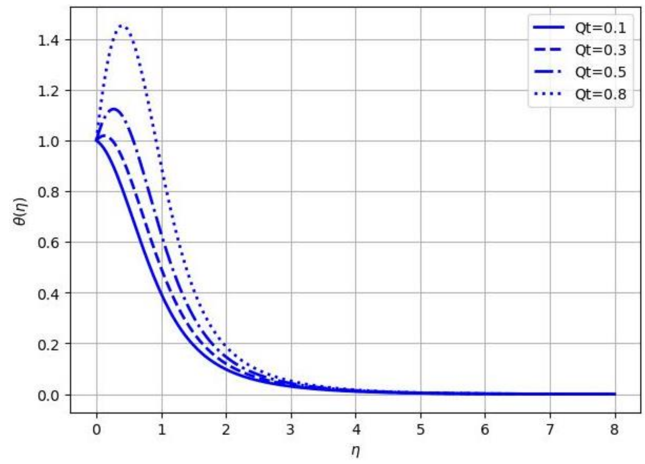

Figure 9. *Influence of* Qt *on* $\theta(\eta)$.

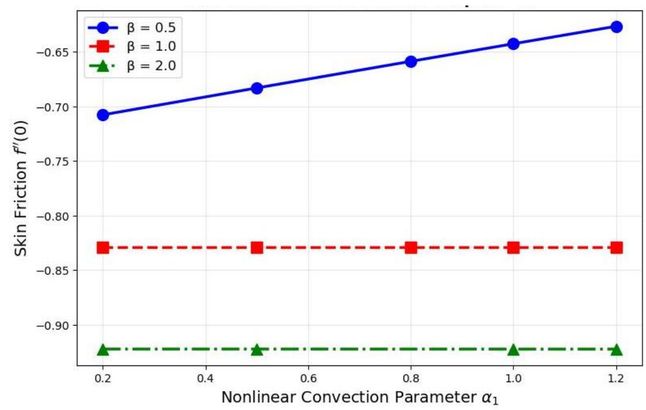

Figure 10. *Influence of* β *and* $\alpha 1$ *on skin friction.*

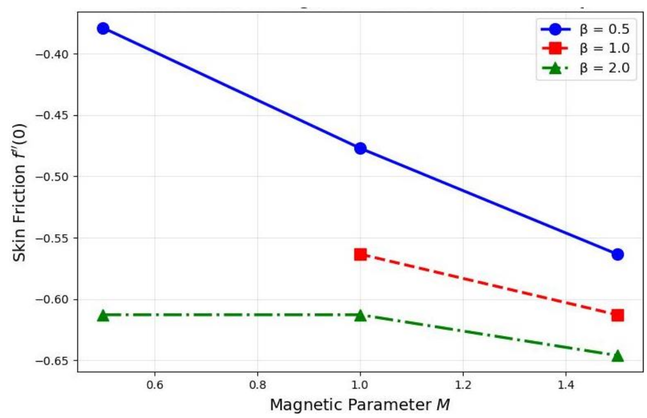

Figure 11. *Influence of* β *and* M *on skin friction.*

4. Conclusion

The present study examined the mixed convective magnetohydrodynamic flow and heat transfer characteristics of a Casson-Williamson fluid over a wedge in the presence of nonlinear thermal buoyancy, thermal radiation, a uniform heat source, and exponential heat generation. The governing nonlinear equations were transformed into a system of ordinary differential equations using similarity transformations and solved numerically by the shooting method coupled with the RK45 algorithm. The principal findings are summarized as follows:

1) Increasing the Casson parameter (β) and Williamson parameter (We) suppresses the fluid velocity, whereas both parameters enhance the temperature distribution by increasing the thermal boundary-layer thickness.
2) The mixed convection parameter (Gr) and the nonlinear convection parameter (α_1) accelerate the fluid motion due to the strengthening of buoyancy forces.
3) The thermal radiation parameter (Rd), uniform heat source parameter (Q_t), and exponential heat generation parameter (Q_E) significantly increase the fluid temperature by supplying additional thermal energy to the boundary layer.
4) The magnitude of the skin-friction coefficient decreases with increasing Casson parameter and magnetic parameter, while the nonlinear convection parameter enhances the wall shear stress, particularly for smaller values of the Casson parameter.
5) The local Nusselt number decreases with increasing thermal radiation parameter, indicating that stronger radiative effects reduce the heat transfer rate from the wedge surface.

Overall, the present investigation demonstrates that the combined effects of non-Newtonian rheology, magnetic field, nonlinear convection, thermal radiation, and internal heat generation substantially influence the momentum and thermal transport characteristics of Casson-Williamson fluids. These results are expected to be useful in the design and optimization of engineering systems involving non-Newtonian electrically conducting fluids, such as polymer extrusion, metallurgical processing, coating technologies, cooling systems, and energy transport applications. Future research may extend the present study to unsteady and three-dimensional flows, variable thermophysical properties, slip boundary conditions, and experimental validation to further improve the applicability of the proposed model to practical engineering problems.

Abbreviations

C_f	Skin-Friction Coefficient
Nu_x	Local Nusselt Number
$RK45$	Runge-Kutta Fourth-Fifth Order

Author Contributions

Doddarasinakere Sreenivasaiah Dhananjaiah: Conceptualization, Resources, Supervision, Validation, Writing – review & editing

Puttaramaiah Prakasha: Data curation, Methodology, Software, Validation, Visualization, Writing – review & editing

Danagur Kalaiah Jyoti: Formal Analysis, Investigation, Software, Visualization, Writing – original draft, Writing – review & editing

Conflicts of Interest

The authors declare no conflicts of interest.

References

[1] Ireka, I. E. (2015). Computational analysis of non-isothermal flow of non-Newtonian fluids. https://doi.org/10.1016/j.jnnfm.2012.11.001

[2] Fatahian, E., Kordani, N., & Fatahian, H. (2018). The application of computational fluid dynamics (CFD) method and several rheological models of blood flow: A review. Gazi University Journal of Science, 31(4), 1213–1227. https://doi.org/10.35378/gujs.706052

[3] Fatahian, E., Kordani, N., & Fatahian, H. (2018). A review on rheology of non-Newtonian properties of blood. IIUM Engineering Journal, 19(1), 237–250. https://doi.org/10.31436/iiumej.v19i1.826

[4] Casson, N. (1959). Flow equation for pigment-oil suspensions of the printing ink-type. In C. C. Mill (Ed.), Rheology of disperse systems (pp. 84–104). Pergamon Press. https://doi.org/10.1515/mt-1959-010903

[5] Mukhopadhyay, S., De, P. R., Bhattacharyya, K., & Layek, G. C. (2013). Casson fluid flow over an unsteady stretching surface. Ain Shams Engineering Journal, 4(4), 933–938. https://doi.org/10.1016/j.asej.2013.04.004

[6] Nandeppanavar, M. M., Vaishali, S., Kemparaju, M., & Raveendra, N. (2020). Theoretical analysis of thermal characteristics of Casson nanofluid flow past an exponential stretching sheet in Darcy porous media. Case Studies in Thermal Engineering, 21, 100717. https://doi.org/10.1016/j.csite.2020.100717

[7] Awais, M., Raja, M. A. Z., Awan, S. E., Shoaib, M., & Ali, H. M. (2021). Heat and mass transfer phenomenon for the dynamics of Casson fluid through porous medium over shrinking wall subject to Lorentz force and heat source/sink. Alexandria Engineering Journal, 60(1), 1355–1363. https://doi.org/10.1016/j.aej.2020.10.056

[8] Walelign, T., Haile, E., Kebede, T., & Walelgn, A. (2020). Analytical study of heat and mass transfer in MHD flow of chemically reactive and thermally radiative Casson nanofluid over an inclined stretching cylinder. Journal of Physics Communications, 4(12), 125003. https://doi.org/10.1088/2399-6528/abcdba

[9] Abo-Dahab, S., Abdelhafez, M., Mebarek-Oudina, F., & Bilal, S. (2021). MHD Casson nanofluid flow over nonlinearly heated porous medium in presence of extending surface effect with suction/injection. Indian Journal of Physics, 96(5), 1301–1315. https://doi.org/10.1007/s12648-020-01923-z

[10] Reddy, B. N., & Maddileti, P. (2023). Casson nanofluid and Joule parameter effects on variable radiative flow of MHD stretching sheet. Partial Differential Equations in Applied Mathematics, 7, 100487. https://doi.org/10.1016/j.padiff.2022.100487

[11] Gubena, T., & Ibrahim, W. (2023). A 3D flow analysis of Casson nanofluid flow over a stretching surface with non-Fourier heat and non-Fick's mass flux. International Journal of Thermofluids, 20, 100488. https://doi.org/10.1016/j.ijft.2023.100488

[12] Ali, M. Y., Reza-E-Rabbi, S., Ahmmed, S. F., Nabi, M. N., Azad, A. K., & Muyeen, S. (2024). Hydromagnetic flow of Casson nanofluid across a stretched sheet in the presence of thermoelectric and radiation effects. International Journal of Thermofluids, 21, 100484. https://doi.org/10.1016/j.ijft.2023.100484

[13] Reddy Gorla, R. S., & Sidawi, I. (1994). Free convection on a vertical stretching surface with suction and blowing. Applied scientific research, 52(3), 247-257. https://doi.org/10.1007/bf00853952

[14] Chamkha, A. J. (1997). Non-Darcy fully developed mixed convection in a porous medium channel with heat generation/absorption and hydromagnetic effects. Numerical Heat Transfer, Part A Applications, 32(6), 653-675. https://doi.org/10.1080/10407789708913911

[15] Hayat, T., Abbas, Z., Pop, I., & Asghar, S. (2010). Effects of radiation and magnetic field on the mixed convection stagnation-point flow over a vertical stretching sheet in a porous medium. International Journal of Heat and Mass Transfer, 53(1-3), 466-474. https://doi.org/10.1016/j.ijheatmasstransfer.2009.09.010

[16] Das, K. (2013). Mixed convection stagnation point flow and heat transfer of Cu-water nanofluids towards a shrinking sheet. Heat Transfer-Asian Research, 42(3), 230-242. https://doi.org/10.1002/htj.21037

[17] Islam, S., Khan, A., Kumam, P., Alrabaiah, H., Shah, Z., Khan, W.,... & Jawad, M. (2020). Radiative mixed convection flow of maxwell nanofluid over a stretching cylinder with joule heating and heat source/sink effects. Scientific reports, 10(1), 17823. https://doi.org/10.1038/s41598-020-74393-2

[18] Tulu, A., Hirpho, M., & Sohail, M. (2024). Modeling and simulation of mixed convection flow with viscous dissipation in a lid-driven hexagonal cavity using finite element method. International Journal of Thermofluids, 22, 100702. https://doi.org/10.1016/j.ijft.2024.100702

[19] Al-Kaby, R. N., Abdulhaleem, S. M., Hameed, R. H., & Yasiry, A. (2025). Mixed convection heat transfer and fluid flow of nanofluid/porous medium under magnetic field influence. Applied Sciences, 15(3), 1087. https://doi.org/10.3390/app15031087

[20] Znaidia, S., Rehman, S., Drissi, N., Asiri, F., & Nasr, S. (2025). Mixed Convection Flow and Heat Transfer of Williamson Drilling Nanofluid Over a Stretching Cylinder Using Brinkman-Maxwell-Garnett Model and temperature-dependent Features. Journal of Nonlinear Mathematical Physics, 32(1), 78. https://doi.org/10.1007/s44198-025-00292-7

[21] Kameswaran, P. K., Sibanda, P., Partha, M. K., & Murthy, P. V. S. N. (2014). Thermophoretic and nonlinear convection in non-Darcy porous medium. Journal of Heat Transfer, 136(4), 042601. https://doi.org/10.1115/1.4025902

[22] Hayat, T., Ullah, I., Alsaedi, A., Waqas, M., & Ahmad, B. (2017). Three-dimensional mixed convection flow of Sisko nanoliquid. International Journal of Mechanical Sciences, 133, 273-282. https://doi.org/10.1016/j.ijmecsci.2017.07.037

[23] Khan, M. I., Khan, T. A., Qayyum, S., Hayat, T., Khan, M. I., & Alsaedi, A. J. T. E. P. J. P. (2018). Entropy generation optimization and activation energy in nonlinear mixed convection flow of a tangent hyperbolic nanofluid. The European Physical Journal Plus, 133(8), 329. https://doi.org/10.1140/epjp/i2018-12093-y

[24] Irfan, M. (2021). Study of Brownian motion and thermophoretic diffusion on non-linear mixed convection flow of Carreau nanofluid subject to variable properties. Surfaces and Interfaces, 23, 100926. https://doi.org/10.1016/j.surfin.2021.100926

[25] Idowu, A. S., Akolade, M. T., Oyekunle, T. L., & Abubakar, J. U. (2021). Nonlinear convection flow of dissipative Casson nanofluid through an inclined annular microchannel with a porous medium. Heat transfer, 50(4), 3388-3406. https://doi.org/10.1002/htj.22033

[26] Ibrahim, W., & Kenea, G. (2024). Nonlinear convection flow of a micropolar nanofluid past a stretching sphere with convective heat transfer. Journal of Nanofluids, 13(2), 407-422. https://doi.org/10.1166/jon.2024.2120

[27] Kenea, G., & Ibrahim, W. (2024). Nonlinear convection stagnation point flow of Oldroyd-B nanofluid with non-Fourier heat and non-Fick's mass flux over a spinning sphere. Scientific Reports, 14(1), 841. https://doi.org/10.1038/s41598-024-51475-z

[28] Reddy, G. S. K., Raju, S. S. K., Mulki, H., & Souayeh, B. (2026). Nonlinear Convection of a Power-Law Fluid-Saturated Reactive Porous Layer. Axioms, 15(7), 487. https://doi.org/10.3390/axioms15070487

[29] R. Cortell, A note on magnetohydrodynamic flow of a power-law fluid over a stretching sheet, Appl. Math. Comput., 168, 557-566 (2005). https://doi.org/10.1016/j.amc.2004.09.046

[30] M. N. Tufail, A. S. Butt and A. Ali, Heat source/sink effects on non-Newtonian MHD fluid flow and heat transfer over a permeable stretching surface: Lie group analysis, Indian. J. Phys., 88, 75-82 (2013). https://doi.org/10.1007/s12648-013-0376-3